VNU Journal of Science: Mathematics - Physics

Journal homepage: https://js.vnu.edu.vn/MaP

Original Article

Effect of pH on Structure and Green Emission of Er/Yb/Mo Tri-doped Hydroxyapatite

Hoang Nhu Van[1,2,*], Nguyen Tien Dung[3], Nguyen Van Hai[3], Cu Van Thai[3], Vu Thi Ngoc Minh[4], Nguyen Xuan Truong[4], Bui Thi Hoan[5], Pham Van Huan[6], Pham Hung Vuong[6]

[1]*Phenikaa University, Yen Nghia, Ha Dong, Hanoi, Vietnam*

[2]*Phenikaa Research and Technology Institute (PRATI), A&A Green Phoenix Group JSC, 167 Hoang Ngan, Trung Hoa, Cau Giay, Hanoi, Vietnam*

[3]*National University of Education, 136 Xuan Thuy, Cau Giay, Hanoi, Vietnam*

[4]*School of Chemical Engineering, Hanoi University of Science and Technology (HUST), 01 Dai Co Viet, Hanoi, Vietnam*

[5]*Thuy Loi University, 175 Tay Son, Dong Da, Hanoi, Vietnam*

[6]*Advanced Institute for Science and Technology, Hanoi University of Science and Technology (HUST), 01 Dai Co Viet, Hanoi, Vietnam*

Received 21 September 2021
Revised 28 October 2021; Accepted 20 November 2021

Abstract: This paper reported the impact of pH on the structure, morphology, and the green upconversion (UC) emission of Er/Yb/Mo tri-doped hydroxyapatite (HA) synthesized through hydrothermal method. X-ray diffraction confirmed that the pH of the solution strongly influenced the phase composition of the phosphors, and HA single phase was obtained at a high pH value. Transmission electron microscopy (TEM) and high-resolution transmission electron microscopy (HRTEM) images of the phosphor exhibited rod-like morphology, and their length increased with increased of the pH values. Under laser-diode excitation wavelength of 975 nm, the phosphor showed typical upconversion emission bands of the Er^{3+} ion: strong green emission bands around 510-535/540-560 nm and weak red emission bands around 630-680 nm. The green and red emission intensity as a function of pH reached its maximum value at pH8. Finally, the emission intensity of

* Corresponding author.
E-mail address: van.hoangnhu@phenikaa-uni.edu.vn

https//doi.org/10.25073/2588-1124/vnumap.4680

the phosphor was not linear dependent on the pH of the solution. The obtained results suggest potential applications of the HA: Er/Yb/Mo phosphors in biomedicine.

Keywords: Hydroxyapatite; Green emission; Hydrothermal method; up-conversion.

1. Introduction

Biomaterials based on Rare-earth (RE) doped hydroxyapatite (HA) are extensively used in biomedical applications such as bioimaging [1], drug delivery [2], bone substitute material [3], biosensor [4], and other fields [5]. This is because these biomaterials exhibit excellent stability thermal, efficient emission, high bioactivity, great biocompatibility, and non-toxicity [1, 6, 7]. HA has three sites of Ca^{2+}, PO_4^{3-}, and OH^- that can be easily replaced by many cations and anions such as Sr^{2+}, Na^+, RE^{3+}, CO_3^{2-}, VO_4^{3-}, F^-, Cl^- [8–11]. The structure, morphology, optical properties, as well as application areas of the RE doped HA, depend on the many synthesis conditions such as synthesis method, Ca/P ratio, dopant ions, pH of the solution, and initial materials, etc. [5, 12–14]. Xie et al. [12] observed the energy transfer from Gd^{3+} to Eu^{3+} of the HA: Eu, Gd phosphor as imaging agents in vitro and in vivo. Dembski et al. [13] reported that the luminescence properties of Eu^{3+}-doped SiO_2/Calcium phosphate core-shell depend on the pH, where they indicate that the formation of a calcium phosphate shell is possible at pH below 4.5 and above 6.5. Furthermore, the cell proliferation test shows that the phosphor can be used in various biological and medical diagnostic applications, particularly as labels for imaging experiments on living cells. Meanwhile, Nayak et al. [14] investigated the synthesis of HA from eggshells and studied the kinetics and mechanism of the fluoride removal process. These obtained results display that the largest efficiency of the fluoride removal was of 96 % at pH 6, owing to the monolayer and multilayer absorption of the fluoride onto the porous HA. Recently, Silva et al. [5] observed that the emission intensity of the Eu^{3+} doped beta-tricalcium phosphate, β-TCP: Eu, (obtained at pH = 5.8) is 20-times larger than HA: Eu (obtained at pH = 10), indicating the pH strongly influences on phase compositions and photoluminescence (PL) properties of the phosphor. It can clearly be seen that the pH of the solution is an important parameter influenced on the characterization of the RE doped HA, especially as luminescence properties of the phosphor. However, the influence of pH on the structure, morphology, and luminescence properties of Er/Yb/Mo doped HA synthesis at low temperature was not explored. Therefore, in this work, we focus on studying the effect of pH on the green UC emission of Er/Yb/Mo-doped HA synthesized by the hydrothermal method. The structure, morphology, and photoluminescent (PL) properties of the phosphor vs the pH solution were fully investigated.

2. Experimental

HA: 1% Er/12% Yb/4% Mo phosphors were prepared through hydrothermal method at the different pH of the solution. The chemicals with high purity such as $Ca(NO_3)_2{\cdot}4H_2O$ (99.9%), $NH_4H_2PO_4$ (99.9%), $Er(NO_3)_3{\cdot}5H_2O$ (99.99%), $Yb(NO_3)_3{\cdot}5H_2O$ (99.99%) and $(NH_4)_6Mo_7O_{24}$ (99.9%) were used for the synthesis of phosphors. The materials were utterly soluble in de-ionized water and obtained Ca^{2+} (0.5M), $H_2PO_4^-$ (0.5M). The content of the Er^{3+}, Yb^{3+}, and Mo^{6+} ions was fixed at 1, 12, and 4% mol, respectively. The solution of the cations was obtained by mixing solution between the Ca^{2+} ion and the dopant ions, $Er^{3+}/Yb^{3+}/Mo^{6+}$, and stirred for 40 min. After slowly adding $H_2PO_4^-$ solution to the mixed (Sr^{2+}, Er^{3+}, Yb^{3+}, and Mo^{6+}) solution and stirring for 30 min. The different pH values of the solution (pH = 6, 8, 10, and 12) were adjusted using ammonia solution. Next, the reaction mixture was transferred to autoclave and heated under the hydrothermal condition at 200 ℃ for 24 h. Finally, the precipitance was vacuum filter and dried at 100 ℃ for 24 h.

Samples used in this work were labeled in Table 1.

Table 1. Sample labeling

Sample	pH values	Label
HA: 1% Er/12% Yb/4%Mo	6	S1
HA: 1% Er/12% Yb/4%Mo	8	S2
HA: 1% Er/12% Yb/4%Mo	10	S3
HA: 1% Er/12% Yb/4%Mo	12	S4

The crystalline structure and the interplanar distances of the crystalline lattice of the synthesized materials was determined by X-ray diffraction patterns using a Bruker D8 Advance X-ray diffractometer and a high-resolution transmission electron microscopy (model JEOL, JEM 2100) technique, respectively. The morphology of the samples was elucidated using a transmission electron microscope (model JEOL, JEM 1010). The PL properties of the materials were investigated using a spectrophotometer (Horiba, USA) equipped with a (975 nm) laser diode as the excitation source. The Gatan Software was used for the analysis of the HRTEM.

3. Results and Discussion

Figure 1 shows the XRD patterns of samples S1, S2, S3, and S4. The results indicated that the structure and phase compositions of the phosphors were strongly dependent on the pH values. At pH6 the phosphor showed three phases: the main dicalcium phosphate (DCP) phase (PDF# 00-002-1351) with triclinic structure (preferred orientation of the {200} plane), β-TCP phase (PDF# 09-0169) with rhombohedral structure, and a small amount of HA phase (PDF# 024-0033) with hexagonal structure. At pH8, the main HA phase was obtained and a small amount of β-TCP and DCP phase. Increases the pH value, the diffraction peaks intensity of the HA phase become stronger, and the diffraction peaks of the TCP phase become weaker, whereas the diffraction peaks of the DCP phase tended to disappear. The highest pH value of 12, the HA single phase was obtained. This phenomenon is due to at low pH value (high H^+ content and low OH^- content), the reaction stops until equation (3) only and the formation of the DCP phase. Meanwhile, at high pH values (high OH^- content and low H^+ content), the reaction continues to equation (5) to form HA. The reactions of the synthesis processes can be written following as:

$$H_2PO_4^- \rightleftharpoons HPO_4^{2-} + H^+ \quad (1)$$

$$HPO_4^{2-} \rightleftharpoons PO_4^{3-} + H^+ \quad (2)$$

$$Ca^{2+} + HPO_4^{2-} \leftrightharpoons CaHPO_4 \quad (3)$$

$$Ca^{2+} + PO_4^{3-} \leftrightharpoons Ca_3(PO_4)_2 \quad (4)$$

$$10CaHPO_4 + 2OH^- \rightleftharpoons Ca_{10}(PO_4)_6(OH)_2 + 10H^+ + 4PO_4^{3-} \quad (5)$$

Interestingly, the diffraction peak intensity attributed to (210) plane of HA phase is strongest, indicating the preferred orientation of the phosphor corresponding to the (210) plane. It becomes weaker with the increase of the pH, The preferred orientation of the (210) plane of HA phase enhanced the UC emission of phosphors as we have reported in a recent work [15]. A high pH value is suitable for the

formation of HA single phase. Many previous works [1, 2, 16] have also obtained similar results. Mansour et al. [17] observed that the dicalcium phosphate dihydrate (DCPD) phase was obtained at below pH7 and HA phase was obtained at above pH7. Liu et al., [11] also studied the influence of pH and temperature on the morphology of HA prepared by the hydrothermal method. They observed that the mixture phases DCP and HA were obtained at lower pH 9, and HA single phase was obtained at pH14, while the morphology of the materials changed from whisker (pH6) to the nanoparticle (pH14). Recently, Silva et al. [5] found that the β-TCP single phase was obtained at pH5.89 and HA single phase was obtained at pH 10.28. As can be seen in the current work and the previous document, the pH of the solution significantly influenced the materials' phase composition. In addition, all samples showed sharp diffraction peaks, suggesting the high crystalline and the successful synthesis of phosphor. The change phase compositions of the phosphor could influence on UC emission intensity of the materials.

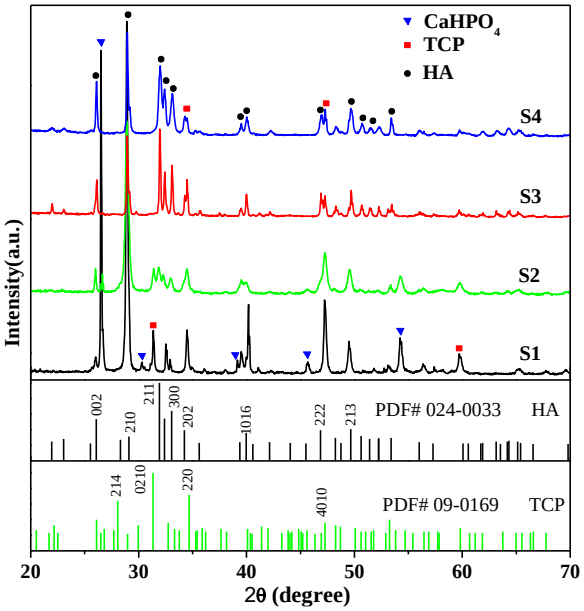

Figure 1. XRD patterns of the S1, S2, S3, and S4 samples.

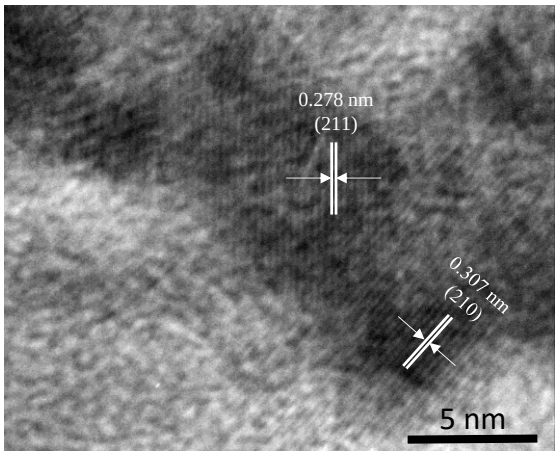

Figure 2. HRTEM image of the S2 sample.

Furthermore, the HRTEM technique was used for analysis the crystalline lattice of the S2 sample, the results were shown in Figure 2. The interplanar distances between the adjacent lattice planes determined from Figure 2 are of 0.307 nm and 0.279 nm, attributed to the lattice spacing $d_{(210)}$, and $d_{(211)}$ of the hexagonal structure, HA: Er/Yb/Mo. The lattice fringes in the HRTEM image (Figure 2) confirmed again the high crystallinity of the sample, which is in good agreement with the data from XRD patterns.

Figure 3 displays TEM images of the materials synthesized at different pH values (namely 6, 8, 10, and 12). It was evident that the significant change the phosphor' morphology (from plate-like to rod-like morphology) when pH of the solution increases from 6 to 12. At pH6 (Figure 3a) the formation of the large agglomerates composed of fine crystallites of the synthesis material were obtained. While at pH8 (Figure 3b), the phosphor showed uniform distribution of the nanoparticle with an average size of about 30 – 50 nm. Interestingly, at pH10 and 12, (Figure 3c and d) the rod-like morphology of the synthesis phosphor was obtained with its' average length about 150 nm and diameter about 20 – 30 nm. These results indicate that the growth and crystallization processes of the phosphor can be controlled by the pH value of the solution. It means that a higher pH value could result in increasing the probability preferred orientation of the nuclear growth corresponds to the c-axis [5, 18–20], leading to obtain the rod-like morphology of the phosphor. The similar results were also observed before in [5, 19, 21]. Van et al. [22] observed that rod-like morphology of HA was obtained for the sample synthesized by co-precipitation method at pH10. Hoai et al. [23] also synthesized HA nanorods through the hydrothermal method at pH values range from 9 to 11. They have confirmed that the morphology of the materials depended significantly on reaction conditions such as pH, hydrothermal time, and surfactant.

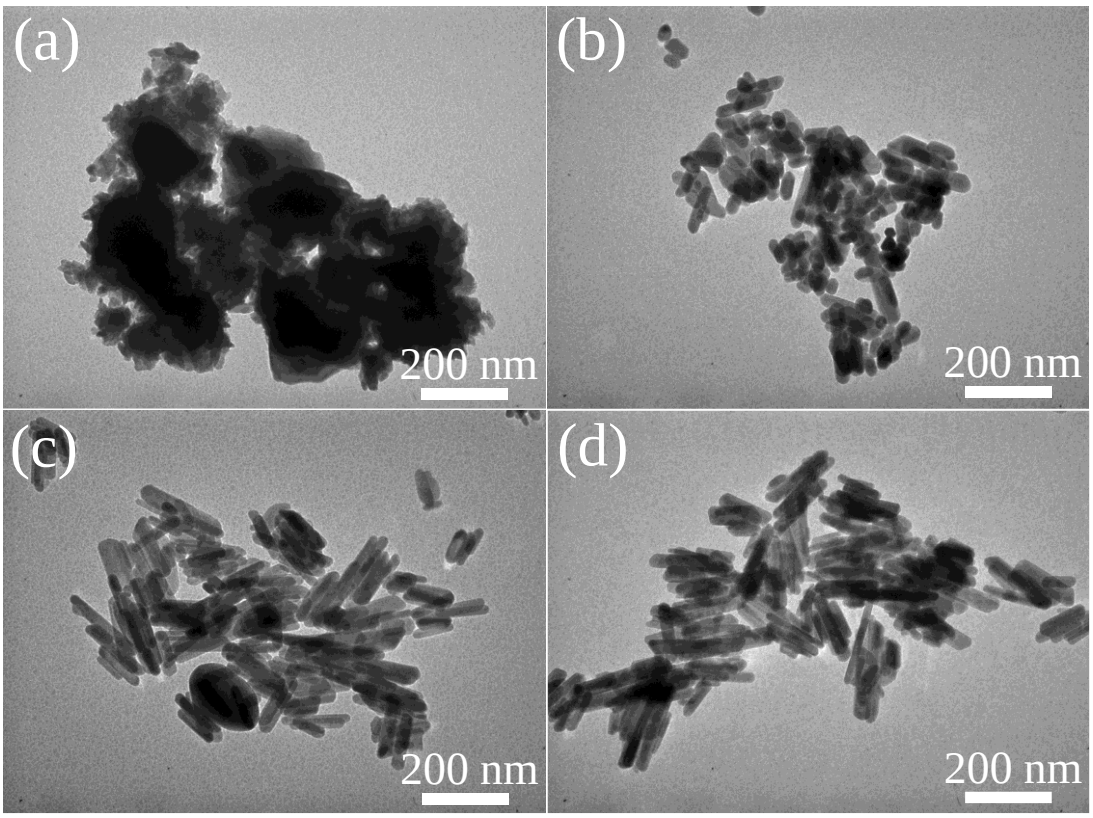

Figure 3. TEM image of the system synthesis at (a) pH6, (b) pH8, (c) pH10, and (d) pH12.

Above-mentioned results indicate that the pH value of the solution was important conditions in the sample synthesis that strongly influenced the morphology of the materials. The changing morphology of the synthesized phosphor caused by the pH of the solution could influence on the UC properties of the phosphor.

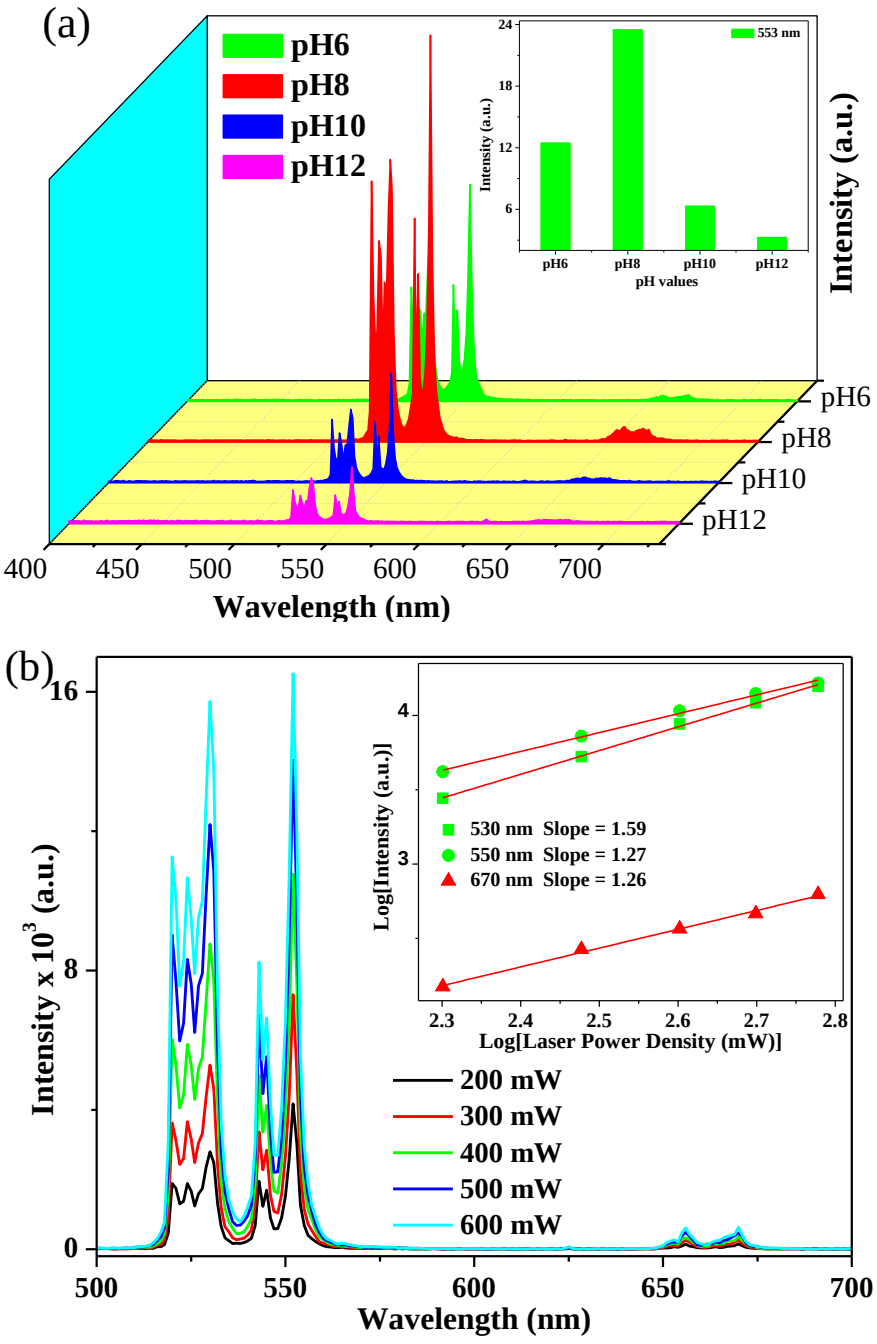

Figure 4. (a) UC emission spectra of the phosphor synthesis at difference pH values and (b) The UC emission spectra of the S2 sample with different power density from 200 mW to 600 mW. The insert of Figure 4b depicts the log – log plots of UC emission intensity as a function of the excitation power density.

Figure 4a exhibits the UC emission spectra of samples S1, S2, S3, and S4. As shown in Figure 4a, all phosphors showed strong green UC emission bands ranging 510–535 nm and 540–560 nm. Meanwhile, the red emission band ranging 640–680 nm was very weak. The green and red emission bands were as a function of the pH values (inset in Figure 4a). The green and red emission bands were attributed to the $^2H_{11/2} \rightarrow {}^4I_{15/2}/{}^4S_{3/2} \rightarrow {}^4I_{15/2}$ and $^4F_{9/2} \rightarrow {}^4I_{15/2}$ transitions of Er^{3+}, respectively. The selective enhancement in green UC emission can be explained due to the energy transfer from the high-energy excitation state of the $Yb^{3+} - MoO_4^{2-}$ dimer to the $^4F_{7/2}$ level of Er^{3+} [24]. It can be seen in the inset of Figure 4, the UC emission intensity of phosphor increased from pH6 to pH8 and reached its maximum value at pH8 then decreased with further increased pH. This can be explained as follows: i) The intense UC emission of the S1 and S2 samples was due to the presence of the β-TCP phase in the systems (Figure 1), leading to increases the UC emission intensity of the phosphor. This phenomenon has also been observed by Silva et al., [5] that they found the emission intensity of TCP: Eu (obtained at low pH, 5.89) was 20-times higher than HA: Eu (obtained at high pH, 10.28); and ii) At high pH values (10 and 12), the presence of the OH^- groups in the HA phase has a luminescence quenching effect [22, 24, 25], leads to decrease UC emission intensity of the phosphor, which has also been explored in our recent work [26]. These results indicate that the UC emission intensity of the phosphor is not linear dependent on the pH of the solution. Along with the HA, β-TCP, and BCP, dicalcium phosphate (DCP) has also been widely studied in many fields of application as coatings of metallic prostheses, self-setting injectable bone cement, and biodegradable scaffolds [27, 28]. Therefore, the S2 sample exhibits strong UC green emission which would be suitable for biomedical applications.

Furthermore, the dependence of the UC emission intensity (I_{uc}) on the excitation power (P_{pump}) was determined, as shown in Figure 4b. It can be described as follows [29]: $I_{uc} \propto (P_{pump})^n$. Where, n is number of absorbed photons per emitted UC photon. It can be seen in Figure 4b, the UC emission intensity is a function of the 975 nm excitation power source. In addition, the slope (n) values (inset in Figure 4b) of the green (530/550 nm) and red (660 nm) emission are 1.59, 1.27, and 1.26, suggesting the two-photon process for both green and red emission in the case of the S2.

4. Conclusion

The influence of pH on the spectral properties of Er/Yb/Mo-doped hydroxyapatite synthesized by the hydrothermal method were investigated. We found that the phase composition, morphology, and photoluminescence properties of the phosphor were strongly influenced by the pH of the solution. Under 975 nm excitation, all phosphors possess a strong green emission and a weak red emission band of the Er^{3+} ion. The largest emission intensity of the synthesized samples was achieved at pH8 This indicated that the presence of the β-TCP phase (obtained at low pH values) in the system leading to improvement efficient emission. Furthermore, the UC emission intensity of the phosphor was not linear dependent on the pH of the solution. The obtained results also indicate that the intense green UC emission of the HA: Er/Yb/Mo materials has potential applications in biomedical fields.

Acknowledgments

This study was funded by the Vietnam National Foundation for Science and Technology Development (NAFOSTED) under grant number 103.03-2019.27.

References

[1] A. Fihri, C. Len, R. S. Varma, and A. Solhy, Hydroxyapatite : A Review of Syntheses , Structure and Applications in Heterogeneous Catalysis, Coord. Chem. Rev, Vol. 347, 2017, pp. 48-76, https://doi.org/10.1016/j.ccr.2017.06.009.

[2] Y. Xu, L. An, L. Chen, H. Xu, D. Zeng, and G. Wang, Controlled Hydrothermal Synthesis of Strontium-Substituted Hydroxyapatite Nanorods and Their Application as a Drug Carrier for Proteins, Adv. Powder Technol, Vol. 29, 2018, pp. 1042-1048, https://doi.org/10.1016/j.apt.2018.01.008.

[3] V. P. Padmanabhan, R. Kulandaivel, S. N. T. S. Nellaiappan, New Core-Shell Hydroxyapatite/um-Acacia Nanocomposites for Drug Delivery and Tissue Engineering Applications, Mater. Sci. Eng. C, Vol. 92, 2018, pp. 685-693, https://doi.org/10.1016/j.msec.2018.07.018.

[4] I. da Silva Brum, J. J. de Carvalho, J. L. da Silva Pires, M. A. A. de Carvalho, L. B. F. dos Santos, C. N. Elias, Nanosized Hydroxyapatite and β-Tricalcium Phosphate Composite: Physico-chemical, Cytotoxicity, Morphological Properties and in Vivo Trial, Sci. Rep, Vol. 9, 2019, pp. 1-10, https://doi.org/10.1038/s41598-019-56124-4.

[5] F. R. O. Silva, N. B. Lima, S. N. Guilhen, L. C. Courrol, A. Helena, A. Bressiani, Evaluation of Europium-doped HA/β -TCP Ratio Fluorescence in Biphasic Calcium Phosphate Nanocomposites Controlled by the pH Value During the Synthesis, J. Lumin, Vol. 180, 2016, pp. 177-182, https://doi.org/10.1016/j.jlumin.2016.08.030.

[6] Y. Zhang, M. Duan, J. Yan, S. Wang, L. Yuan, Morphology, Structure Evolution and Site-Selective Occupancy of Eu^{3+} in $Ca_{10}(PO_4)_6(OH)_2$ Nanorods Synthesized via Subcritical Hydrothermal Method, Chem. Select, Vol. 3, 2018, pp. 7749-7756, https://doi.org/10.1002/slct.201801362.

[7] Y. Lei, Z. Xu, Q. Ke, W. Yin, Y. Chen, C. Zhang, Y. Guo, Strontium Hydroxyapatite/Chitosan Nanohybrid Scaffolds with Enhanced Osteoinductivity for Bone Tissue Engineering, Mater. Sci. Eng. C, Vol. 72, 2017, pp. 134-142, http:/doi.org/10.1016/j.msec.2016.11.063.

[8] J. F. Cawthray, A. L. Creagh, C. A. Haynes, C. Orvig, Ion Exchange in Hydroxyapatite with Lanthanides, Inorganic Chemistry, Vol. 54, 2015, pp. 1440-1445, https://doi.org/10.1021/ic502425e.

[9] A. Szczes, L. Holysz, E. Chibowski, Synthesis of Hydroxyapatite for Biomedical Applications, Adv. Colloid Interface Sci, Vol. 249, 2017, pp. 321-330, https://doi.org/10.1016/j.cis.2017.04.007.

[10] K. Suchanek, A. Bartkowiak, M. Perzanowski, M. Marszałek, from Monetite Plate to Hydroxyapatite Nanofibers by Monoethanolamine Assisted Hydrothermal Approach, Sci. Rep, Vol. 8, 2018, pp. 15408, https://doi.org/10.1038/s41598-018-33936-4.

[11] J. Liu, X. Ye, H. Wang, M. Zhu, B. Wang, H. Yan, The Influence of pH and Temperature on the Morphology of Hydroxyapatite Synthesized by Hydrothermal Method, Vol. 29, 2003, pp. 629-633, https://doi.org/10.1016/S0272-8842(02)00210-9.

[12] Y. Xie, W. He, F. Li, T. S. H. Perera, L. Gan, Y. Han, X. Wang, S. Li, H. Dai, Luminescence Enhanced Eu^{3+}/Gd^{3+} Co-Doped Hydroxyapatite Nanocrystals as Imaging Agents In Vitro and In Vivo, ACS Applied Materials & Interfaces, Vol. 8, 2016, pp. 10212-10219, https://doi.org/10.1021/acsami.6b01814.

[13] S. Dembski, M. Milde, M. Dyrba, S. Schweizer, C. Gellermann, Effect of pH on the Synthesis and Properties of Luminescent SiO_2/Calcium Phosphate : Eu^{3+} Core-Shell Nanoparticles, Langmuir, Vol. 27, 2011, pp. 14025-14032, https://doi.org/10.1021/la2021116.

[14] B. Nayak, A. Samant, R. Patel, P. K. Misra, Comprehensive Understanding of the Kinetics and Mechanism of Fluoride Removal over a Potent Nanocrystalline Hydroxyapatite Surface, ACS. Omega, Vol. 2, 2017, pp. 8118-8128, https://doi.org/10.1021/acsomega.7b00370.

[15] H. N. Van, L. M. Tu, D. T. T. Dung, P. H. Vuong, N. D. Hung, P. T. H. Diep, H. V. Hung, On Enhancement and Control of Green Emission of Rare Earth Co-Doped Hydroxyapatite Nanoparticles: Synthesis and Upconversion Luminescence Properties, New J. Chem, Vol. 45, 2021, pp. 751-760, https://doi.org/10.1039/D0NJ04847J.

[16] D. T. T. Dung, V. T. N. Minh, N. X. Truong, P. V. Huan, P. H. Vuong, N. D. Hung, B. T. Hoan, L. M. Tu, H. N. Van, Dual-mode Green Emission and Temperature Sensing Properties of Rare-Earth-Element-Doped Biphasic Calcium Phosphate Composites, J. Alloys Compd, Vol. 871, 2021, pp. 159483, https://doi.org/10.1016/j.jallcom.2021.159483.

[17] S. F. Mansour, S. I. El-dek, M. A. Ahmed, S. M. A. Elwahab, M. K. Ahmed, Effect of Preparation Conditions on the Nanostructure of Hydroxyapatite and Brushite Phases, Appl. Nanosci, Vol. 6, 2016, pp. 991-1000, https://doi.org/10.1007/s13204-015-0509-4.

[18] K. Lin, J. Chang, R. Cheng, M. Ruan, Hydrothermal Microemulsion Synthesis of Stoichiometric Single Crystal Hydroxyapatite Nanorods with Mono-dispersion and Narrow-size Distribution, Mater. Lett, Vol. 61, 2007, pp. 1683-1687, https://doi.org/10.1016/j.matlet.2006.07.099.

[19] F. Ren, Y. Leng, Y. Ding, K. Wang, Hydrothermal Growth of Biomimetic Carbonated Apatite Nanoparticles with Tunable Size, Morphology and Ultrastructure, CrystEngComm, Vol. 15, 2013, pp. 2137-2146, https://doi.org/10.1039/C3CE26884E.

[20] A. J. Nathanael, D. Mangalaraj, S. I. Hong, Y. Masuda, Synthesis and in-Depth Analysis of Highly Ordered Yttrium Doped Hydroxyapatite Nanorods Prepared by Hydrothermal Method and Its Mechanical Analysis, Mater. Charact, Vol. 62, 2011, pp. 1109-1115, https://doi.org/10.1016/j.matchar.2011.09.008.

[21] F. Chen, Y. J. Zhu, X. Y. Zhao, B. Q. Lu, J. Wu, Solvothermal Synthesis of Oriented Hydroxyapatite Nanorod/Nanosheet Arrays using Creatine Phosphate as Phosphorus Source, CrystEngComm, Vol. 15, 2013, pp. 4527-4531, https://doi.org/10.1039/C3CE40115D.

[22] H. N. Van, P. D. Tam, N. D. T. Kien, P. T. Huy, P. H. Vuong, Enhancing the Luminescence of Eu^{3+}/Eu^{2+} Ion-Doped Hydroxyapatite by Fluoridation and Thermal Annealing, Luminescence, Vol. 32, 2017, pp. 817-823, https://doi.org/10.1002/bio.3257.

[23] T. T. Hoai, N. K. Nga, L. T. Giang, T. Q. Huy, P. N. M. Tuan, B. T. T. Binh, Hydrothermal Synthesis of Hydroxyapatite Nanorods for Rapid Formation of Bone-Like Mineralization, J. Electron. Mater, Vol. 46, 2017, pp. 5064-5072, https://doi.org/10.1007/s11664-017-5509-6.

[24] H. N. Van, V. N. Hung, P. H. Vuong, P. V. Huan, B. T. Hoan, N. D. Hung, L. M. Tu, A Novel Upconversion Emission Material Based on Er^{3+}-Yb^{3+}-Mo^{6+} Tridoped Hydroxyapatite/Tricalcium Phosphate (HA/β-TCP), J. Alloys Compd, Vol. 827, 2020, pp. 154288, http:/doi.org/10.1016/j.jallcom.2020.154288.

[25] G. Gonzalez, C. C. Vera, L. J. Borrero, D. Soto, L. Lozada, J. I. Chango, J. C. Diaz, L. Lascano, Effect of Carbonates on Hydroxyapatite Self-Activated Photoluminescence Response, J. Lumin, Vol. 19, 2018, pp. 385–395. https://doi.org/10.1016/j.jlumin.2017.11.058.

[26] P. H. Vuong, H. N. Van, P. D. Tam, H. N. T. Ha, A Novel 1540 nm Light Emission from Erbium Doped Hydroxyapatite/β-Tricalcium Phosphate through Co-precipitation Method, Mater. Letter, Vol. 167, 2016, pp. 145-147, http:/doi.org/10.1016/j.matlet.2016.01.002.

[27] S. Dorozhkin, Nanodimensional and Nanocrystalline Apatites and other Calcium Orthophosphates in Biomedical Engineering, Biology and Medicine, Materials, Vol. 2, 2009, pp. 1975-2045, https://doi.org/10.3390/ma2041975.

[28] F. Tamimi, Z. Sheikh, J. Barralet, Dicalcium Phosphate Cements: Brushite and Monetite, Acta Biomater, Vol. 8, 2012, pp. 474-487, http:/doi.org/10.1016/j.actbio.2011.08.005.

[29] Y. Zhang, B. Wang, Y. Liu, G. Bai, Z. Fu, H. Liu, Upconversion Luminescence and Temperature Sensing Characteristics of Yb^{3+}/Tm^{3+}:$KLa(MoO_4)_2$ phosphors**,** Dalton Trans, Vol. 50, 2021, pp. 1239-1245.